ACS Catalysis

pubs.acs.org/acscatalysis Research Article

In Situ Identification of Non-Specific Adsorption of Alkali Metal Cations on Pt Surfaces and Their Catalytic Roles in Alkaline Solutions

Li Jiao, Ershuai Liu, Sanjeev Mukerjee, and Qingying Jia*

Cite This: *ACS Catal.* 2020, 10, 11099–11109 Read Online

ACCESS | Metrics & More | Article Recommendations | Supporting Information

ABSTRACT: Alkali metal cations (AM^+) have profound influences on catalytic activities of platinum (Pt) in aqueous solutions, but the underlying mechanisms remain unclear mainly because of limited knowledge of the interactions between AM^+ and Pt surfaces within the interface. Herein, in situ X-ray absorption spectroscopy (XAS) coupled with ab initio FEFF calculations rule out specific adsorption of AM^+ and hydroxyl (OH_{ad}) but not interfacial water with the oxygen facing toward the Pt surface ($H_2O{\downarrow}_{ad}$) within the hydrogen underpotential deposition (H_{UPD}) potential region in alkaline solutions. We further show that AM^+ greatly affects the H_{UPD} peaks and the kinetics of the hydrogen evolution/oxidation reactions (HER/HOR) of Pt in alkaline solutions. We accordingly propose that $H_2O{\downarrow}_{ad}$ is specifically adsorbed on undercoordinated Pt surfaces and bonded with the water molecules coordinated to AM^+, forming the sandwich structure of $Pt{-}H_2O{\downarrow}_{ad}{\cdots}[(H_2O)_x{-}AM]^+$ across the interface; and the exchange between the $H_2O{\downarrow}_{ad}{\cdots}[(H_2O)_x{-}AM]^+$ and H_{ad} yields the sharp H_{UPD} peaks. The AM^+ weakens the $Pt{-}H_2O{\downarrow}_{ad}$ bond via noncovalent interactions and in turn positively shifts the H_{UPD} peaks and hinders the HOR by delaying the oxidative removal of H_{ad}. The AM^+ promotes the HER of Pt by facilitating the removal of the OH_{ad} in the form of $OH_{ad}{\cdots}[(H_2O)_x{-}AM]^+$ subsequent to the dissociation of $H_2O{\downarrow}_{ad}$.

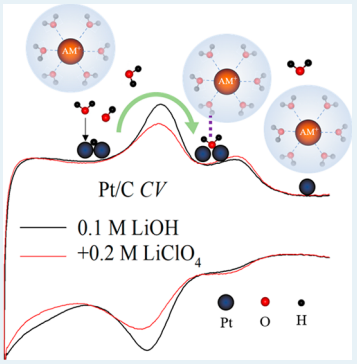

KEYWORDS: *alkali metal cations, specific adsorption, interfacial water, Pt cyclic voltammetry, HER/HOR, XAS*

1. INTRODUCTION

When studying the electrochemistry of platinum (Pt) electrodes in acidic solutions, a dilute $HClO_4$ electrolyte is a common choice owing to the minimal interaction between the Pt surface and ClO_4^- ions within the potential range of 0−1 V versus a reversible hydrogen electrode (RHE). In contrast, HCl and H_2SO_4 have rarely been the choice since both Cl^- and SO_4^{2-} actively interact with Pt surfaces.[1] Likewise, when studying the electrochemistry of Pt electrodes in alkaline solutions, it is critical to recognize whether and how alkali metal cations (AM^+) such as Li^+, Na^+, or K^+ interact with Pt surfaces under reactive conditions. However, this topic has remained unclear, leaving the foundation of alkaline electrochemistry unsound.

The need to understand the interactions between AM^+ and Pt surfaces is manifested by the profound influences of AM^+ on the electrochemical behaviors of Pt electrodes even in dilute alkaline solutions. For instance, Markovic's group reported that when changing the alkaline solution from 0.1 M KOH to 0.1 M LiOH, the kinetics of the hydrogen evolution and oxidation reactions (HER/HOR) of stepped Pt surfaces such as Pt(110) improves markedly; however, that of the Pt(111) remains unchanged.[2] On the contrary, the kinetics of the oxygen reduction reaction (ORR) of both stepped Pt and Pt(111) surfaces slows down dramatically as the electrolyte switches from 0.1 M KOH to 0.1 M LiOH.[2] On the basis of these experimental observations, Markovic et al.[3,4] proposed there exist noncovalent interactions between hydrated alkali metal cations $[(H_2O)_x{-}AM]^+$ and adsorbed OH (OH_{ad}) species on Pt surfaces, and the interactions increase with increasing hydration energies of the AM^+ ($K^+ < Li^+$). In other words, the AM^+ is nonspecifically adsorbed onto Pt surfaces without direct $Pt{-}AM^+$ interactions, and the AM^+ affects the catalytic activity of Pt via affecting the $Pt{-}OH_{ad}$ binding energy indirectly. One merit of this hypothesis is that the absence of the AM^+ effects on the HER/HOR kinetics of Pt(111) can be explained as the OH_{ad} is absent on Pt(111) within the HER/HOR kinetic potential region (<0.3 V) but can be present on stepped Pt surfaces. Within the ORR potential region (>0.7 V), the Pt(111) is covered by OH_{ad} that triggers the AM^+ effects via noncovalent interactions. Recently, we proposed that the AM^+ affects the HER kinetics of undercoordinated Pt surfaces that include both stepped facets and corners, edges, apex, and so on via the noncovalent interaction between $[(H_2O)_x{-}AM]^+$ and OH_{ad} generated from water dissociation

Received: June 24, 2020
Revised: August 6, 2020
Published: August 31, 2020

https://dx.doi.org/10.1021/acscatal.0c02762
ACS Catal. 2020, 10, 11099−11109

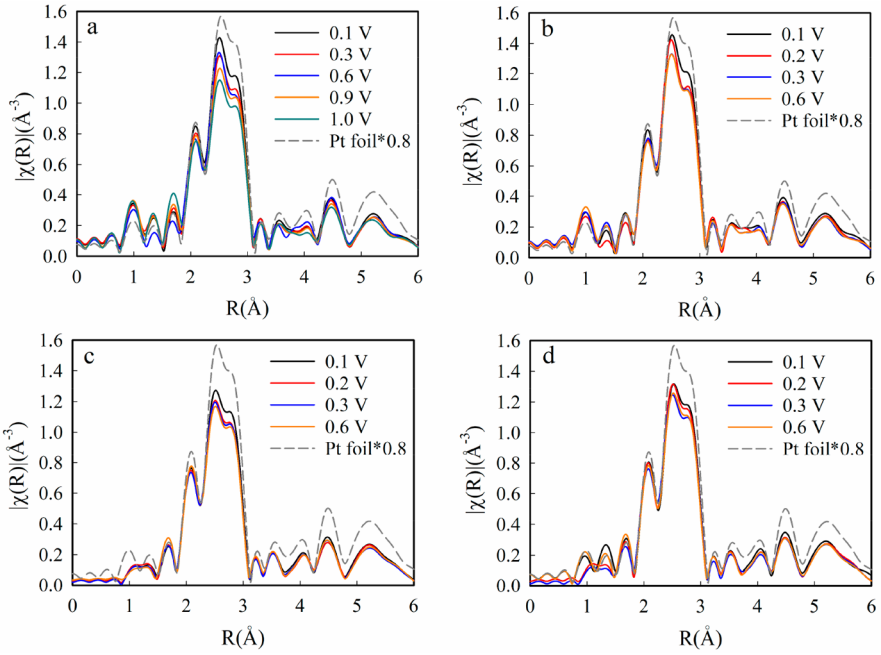

Figure 1. Pt L_3-edge FT-EXAFS spectra of Pt/C collected in an Ar-saturated electrolyte of (a) 0.1 M $HClO_4$, (b) 0.1 M NaOH, (c) 0.1 M NaOH + 0.1 M $NaClO_4$, or (d) 0.1 M NaOH + 0.4 M $NaClO_4$ at various potentials. The FT-EXAFS spectrum of the Pt reference foil with the intensity scaled by 0.8 is also displayed for comparison purpose.

($Pt\text{-}OH_{ad}\cdots[(H_2O)_x\text{–}AM]^+$) as per the hard–soft acid–base (HSAB) mechanism,[5] which is also based on the nonspecific adsorption of hydrated AM^+ on Pt surfaces. However, the presence of OH_{ad} on undercoordinated Pt surfaces within the underpotential deposition of hydrogen (H_{UPD}) potential region in alkaline solutions, which is the basis for the noncovalent interactions between the $[(H_2O)_x\text{–}AM]^+$ and OH_{ad}, has been under extensive debate.[6,7] It is predicted to be possible by density functional theory (DFT) calculations[8] but disproved by microkinetic modeling.[9] Experimentally, it is supported by infrared reflection absorption spectroscopy[10] but not by CO stripping.[11,12]

In contrast, Koper et al.[8,13] proposed that the AM^+ is specifically adsorbed onto the stepped Pt surfaces together with OH_{ad}, in an attempt to explain the AM^+ effects on the cyclic voltammetry (CV) of Pt surfaces in aqueous solutions with a wide pH range of 1–13. They proposed the sharp H_{UPD} peaks of stepped Pt surfaces such as Pt(110) are caused by the exchange between H_{ad} and the OH_{ad} that is coadsorbed on stepped Pt surfaces with AM^+.[8,13] In addition, they showed by density functional theory (DFT) calculations that the specifically adsorbed AM^+ positively shifts the H_{UPD} peaks to higher potentials by weakening the $Pt\text{–}OH_{ad}$ bond, which fully accounts for the non-Nernstian pH shift of the H_{UPD} peaks of stepped Pt surfaces. On the other hand, the absence of the specifically coadsorbed AM^+ and OH_{ad} on the Pt(111) surface accounts for the absence of sharp H_{UPD} peaks and their regular Nernstian pH shift. However, the specific adsorption of AM^+ on undercoordinated Pt surfaces within the H_{UPD} potential region has not been observed experimentally. In contrast, Xu et al.[14] recently ruled out specific adsorption of AM^+ on Pt surfaces based on the combined experiments of CVs and surface enhanced spectroscopy. They alternatively proposed that the non-Nernstian pH shift of the H_{UPD} peaks of stepped Pt surfaces is caused by the pH-dependent structure of interfacial water.[14] Although this hypothesis drops the requirement of specific adsorption of AM^+ and OH_{ad} on stepped Pt surfaces, it has not accounted for the profound influences of AM^+ on the CV features and catalytic activities of Pt surfaces.

We recognize from the contradictory hypothesis briefed above that AM^+ plays important roles in the electrochemical behaviors of Pt in alkaline solutions, but the specific roles remain elusive due largely to the poor understanding of the interactions between AM^+ and Pt surfaces under in situ electrochemical conditions. This recognition drives us to probe the interactions between AM^+ and Pt surfaces in aqueous solutions with varying concentrations of AM^+ within the relevant potential region by means of electrochemical and in situ X-ray absorption spectroscopy (XAS) methods. XAS detects neighboring atoms (AM^+ here) around the absorbing atom (Pt here) based on the interference between the outgoing and backscattering waves in association with the photoelectrons emitted by the absorbing atom and back-scattered by neighboring atoms, respectively. It is thus a suitable technique to identify the $Pt\text{–}AM^+$ interactions in situ because the specifically adsorbed heavy AM^+ such as Na^+ will be detected by XAS once its abundance exceeds the detecting limits of XAS, whereas the nonspecifically adsorbed AM^+ is invisible by XAS since it is located far away from the Pt with H_2O and/or OH_{ad} in between. We were previously able to identify the specifically adsorbed species such as Cl^-,[15] SO_4^{2-},[1,15] OH,[16] and H[17] on Pt surfaces under in situ electrochemical conditions by coupling ab initio FEFF calculations[18] to the $\Delta\mu$ technique. The $\Delta\mu$ is a surface sensitive technique pioneered by Ramaker et al.[17] that is based on extracting the differences of the X-ray absorption near-edge structure (XANES) spectra collected at different potentials. Herein, direct $Pt\text{–}Na^+$ interactions are not observed by in situ XAS in NaOH solutions with the Na^+ concentration up to 0.5 M within 0.1–0.6 V (all potentials here are versus RHE), which rules out specific adsorption of Na^+ on Pt surfaces in

https://dx.doi.org/10.1021/acscatal.0c02762
ACS Catal. 2020, 10, 11099–11109

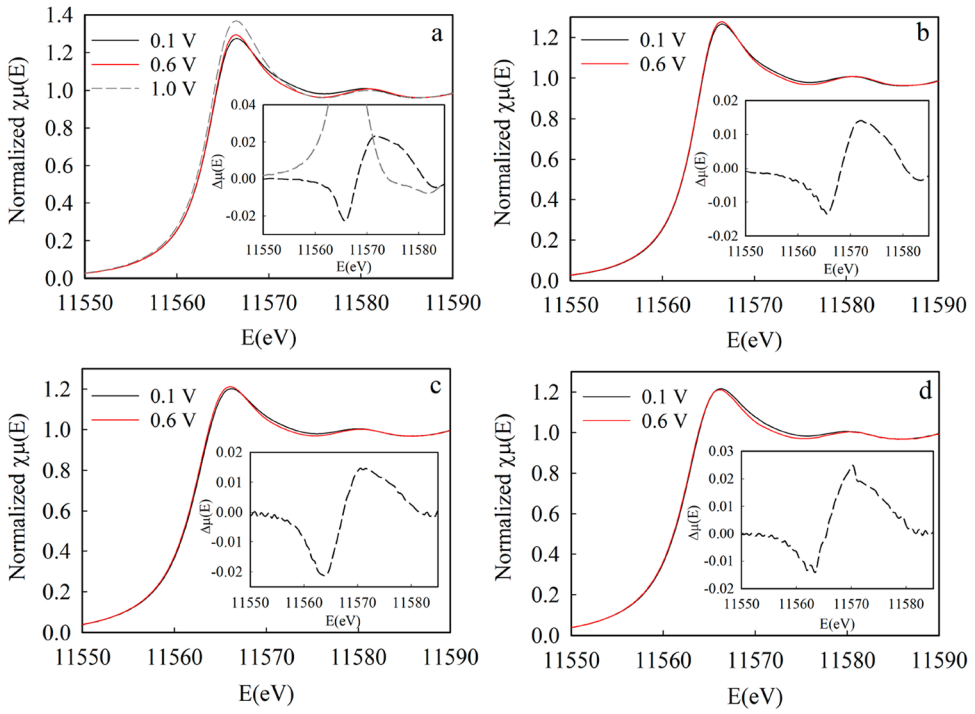

Figure 2. Pt L_3-edge XANES spectra of Pt/C collected in Ar-saturated (a) 0.1 M $HClO_4$, (b) 0.1 M NaOH; (c) 0.1 M NaOH + 0.1 M $NaClO_4$, or (d) 0.1 M NaOH + 0.4 M $NaClO_4$ at various potentials. Experimental $\Delta\mu$ signals derived from the XANES spectra are displayed in the inset.

alkaline solutions. The in situ XAS suggests specific adsorption of interfacial water with the oxygen pointing toward the Pt surfaces (denoted as $H_2O{\downarrow}_{ad}$). We further show that the profound effects of AM^+ on the CV and HER/HOR activities of the Pt electrode can be accounted for by the noncovalent interactions between the $[(H_2O)_x{-}AM]^+$ and $Pt{-}H_2O{\downarrow}_{ad}$ or $Pt{-}OH_{ad}$.

2. RESULTS

2.1. In Situ X-ray Absorption Spectroscopy Studies.

We conducted in situ XAS on Pt/C (Tanaka Kikinzoku Kogyo, 47.2 wt %, ~3 nm) in an Ar-saturated 0.1 M $HClO_4$ electrolyte and 0.1 M NaOH electrolyte with varying concentration of $NaClO_4$ up to 0.4 M. The XAS spectra were collected at the Pt L_3-edge as a function of applied potentials ranging from 0.1 to 1.0 V in acid and 0.1−0.6 V in alkaline. A lower upper potential limit of 0.6 V was chosen for alkaline to avoid Pt dissolution.[19] The in situ Fourier Transform of the extended X-ray absorption fine structure (FT-EXAFS) spectra of Pt in various solutions are displayed in Figure 1. For all cases, the FT-EXAFS spectra are essentially reminiscent of that of the Pt reference foil but with lower intensities of the Pt−Pt scattering peaks (Figure 1), owing to the small size of Pt/C (~3 nm) nanoparticles enriched with undercoordinated Pt atoms. In addition, all the first-shell FT-EXAFS spectra can be well fitted with a pure Pt cluster model (Figure S1 and Table S1). These results confirm that direct Pt−Na interactions are not observed by FT-EXAFS with the Na^+ concentration up to 0.5 M. Meanwhile, the $Pt{-}OH_{ad}$ interaction is observed at 1.0 V in 0.1 M $HClO_4$, as shown by the increase in the intensity of the Pt−O scattering peak around 1.7 Å (Figure 1a). It is also reflected by the concurrent decrease of the intensity of the Pt−Pt scattering peaks centered at 2.4 Å as this is caused by the blocking of the Pt−Pt scattering by the O_{ad} and/or OH_{ad} $(O(H)_{ad})$.[16]

The intensity of the major FT-EXAFS peaks of Pt/C generally increases with decreasing potentials and reaches the highest at 0.1 V in all four electrolytes (Figure 1). The higher peak intensity and correspondingly the higher coordination numbers of Pt/C within the H_{UPD} potential region versus the double layer potential region (0.5−0.7 V) were previously reported by Ramaker et al.[17] They attributed the phenomenon to H_{ad} that makes the Pt particles more spherical and in turn increases the coordination number and the Pt−Pt scattering peak intensity. Alternatively, it can be explained as the Pt−Pt scattering is being blocked by oxygen species within the whole potential range of 0.1−1.0 V but not just at elevated potentials (>0.7 V). By this speculation, the Pt−Pt peak intensity gradually increases as the oxygen coverage gradually reduces with decreasing potential. This speculation is in line with the arguments that the adsorption of OH_{ad} can start as low as 0.1 V on stepped Pt surfaces.[10,13] The specifically adsorbed $H_2O{\downarrow}_{ad}$ is another possible oxygen adsorbate.[20] Because the Pt−O bond is not observed by FT-EXAFS below 0.6 V, which is probably due to the low sensitivity of FT-EXAFS, we apply XANES and $\Delta\mu$ analysis that are more sensitive to adsorbates to probe the identity of surface adsorbates and their configuration in situ.

In situ XANES spectra of the Pt/C in NaOH electrolytes with varied concentrations of Na^+ are displayed in Figure 2. The corresponding $\Delta\mu$ spectra ($\Delta\mu(U) = \mu(U) - \mu(0.6\ V)$ where U represents applied potentials) are displayed in the insets. The XAENS at 0.6 V is chosen as the baseline spectrum because 0.6 V is within the double layer region and the Pt surface has been traditionally assumed to be free of OH_{ad} and H_{ad}. The full set of spectra collected at more potentials is given in Figure S2. In parallel, we employ the FEFF9 code[21] to calculate the XANES spectra based on the Janin's cluster of Pt_6[22] with or without an adsorbate (A_d) located at the atop, bridge, or face centered cubic (fcc) site. The calculated

https://dx.doi.org/10.1021/acscatal.0c02762
ACS Catal. 2020, 10, 11099−11109

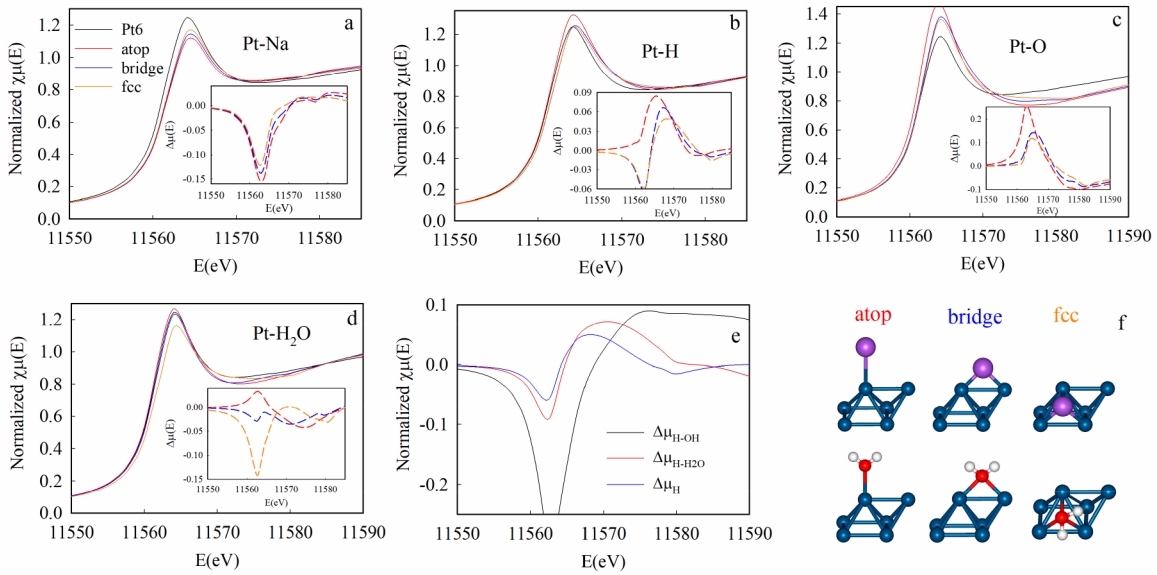

Figure 3. XANES spectra of the Pt_6 cluster with (a) Na, (b) H, (c) O, (d) $H_2O\downarrow_{ad}$, located in the atop, bridge, or fcc site calculated by the FEFF9 code, with the corresponding $\Delta\mu$ signals displayed in the insets. (e) The calculated spectra of $\Delta\mu_{H-OH}$, $\Delta\mu_{H-H_2O}$, and $\Delta\mu_H$. (f) schematic illustration of the Pt_6 cluster with an adsorbate in the atop, bridge, or fcc site. The blue, purple, red, and white balls represent Pt, Na, O, and H atoms, respectively.

XANES spectra are displayed in Figure 3, and the corresponding $\Delta\mu$ spectra ($\Delta\mu = \mu(Pt_6{-}A_d) - \mu(Pt_6)$) are displayed in the insets. Four adsorbate species including H, O (O and OH give essentially the same signal),[16] Na, and $H_2O\downarrow$ are chosen for calculations to cover relevant adsorbates. The H_2O with the H binding to the Pt that represents the H_2O with the H facing toward the Pt electrode ($H_2O\uparrow_{ad}$) is not included since the Pt−H bond is too long (>3 Å)[23] to be detectable by XAS. We stress that the FEFF calculations are not to quantitatively fit the experimental XANES spectra based on the simplified Pt_6 cluster model but to identify the nature of adsorbate and its binding configuration by comparing the adsorbate-induced change of the calculated XANES spectra with the adsorbate-induced difference of experimental XANES spectra collected at different potentials.

As in the case of 0.1 M $HClO_4$ without the presence of Na^+, the white line intensity of the major XANES peak around 11566 eV is higher at 1.0 V than at 0.6 V (Figure 2a), which is caused by the adsorption of $O(H)_{ad}$ at 1.0 V. The electron transfer from the Pt surface to $O(H)_{ad}$ increases the d-band vacancy of Pt and in turn increases the white line intensity that is associated with the transition of electrons from the 2p orbital to the unoccupied 5d orbital.[16] In parallel, adding one oxygen atom onto the Pt_6 cluster increases the Pt white line intensity as well (Figure 3c), and the $\Delta\mu$ spectra closely mimic the $\Delta\mu$(1.0 V). The experimental $\Delta\mu$(1.0 V) and the corresponding FEFF simulations agree well with previous $\Delta\mu$ studies,[16,24] verifying that the oxygen adsorbate can be readily detected by XANES and $\Delta\mu$ spectra.

However, no Na^+ is observed by XANES and $\Delta\mu$ in the alkaline solutions with the Na^+ concentration up to 0.5 M, despite that Na is bigger and heavier than O. In all three alkaline electrolytes, the XANES and $\Delta\mu$ spectra closely resemble those of Pt/C in acid (Figure 2) and those of Pt/C in 0.1 M KOH reported previously,[25] signifying a Pt surface with only H_{ad} at lower potentials. On the other hand, the white line intensity of the calculated XANES spectrum of the Pt_6 cluster drops dramatically upon addition of a Na atom in either atop, bridge, or fcc site, resulting in a prominent dip in the corresponding $\Delta\mu$ spectra (Figure 3a). The significant mismatch between the calculated spectra and the experimental ones rules out specific adsorption of Na^+ in alkaline solutions with the Na concentration up to 0.5 M. This result corroborates the absence of the Pt−Na interactions in the corresponding FT-EXAFS spectra (Figure 1). We therefore conclude that the AM^+ is not specifically adsorbed on Pt surfaces within the H_{UPD} region in alkaline solutions with the AM^+ concentration up to 0.5 M, in line with the recent study by Xu et al.[14] This result is not surprising as the solvation energy of AM^+ is typically much higher than that for electrostatic adsorption, inhibiting the specific adsorption of AM^+.[26]

Next, we examine the presence of H_{ad} within the H_{UPD} potential region based on the XAENS and $\Delta\mu$ results. Although the $\Delta\mu$ spectra of the Pt/C in all the four electrolytes displayed in Figure 2 exhibit a similar s-shape feature, the origins of the s-shape feature are different. The dip of the $\Delta\mu$(0.1 V) spectrum of the Pt/C in 0.1 M NaOH plus 0.4 M $NaClO_4$ is mainly caused by the positive shift of the XANES spectrum toward higher energies when shifting from 0.6 to 0.1 V. Meanwhile the XANES spectrum becomes wider and its white line intensity remains unchanged (Figure 2d). Consequently, the dip of the $\Delta\mu$(0.1 V) is centered around 11563 eV. In perfect agreement with these observations, the XANES spectrum of the Pt nanoclusters with adsorbed H_2 gas in comparison to under vacuum environment also (i) shifts positively; (ii) becomes wider; and (iii) its white line intensity remains unchanged, and consequently, the dip of the corresponding $\Delta\mu$ spectrum is centered around 11563 eV.[27,28] All three occurrences are also observed when putting the H atom onto the Pt_6 cluster in the bridge or fcc site (Figure 3b) and can be explained by the charge transfer from the Pt surface to H_{ad}.[17,28] Since the bridge binding configuration of H_{ad} on Pt surfaces is not supported by literature,[17] we

https://dx.doi.org/10.1021/acscatal.0c02762
ACS Catal. 2020, 10, 11099−11109

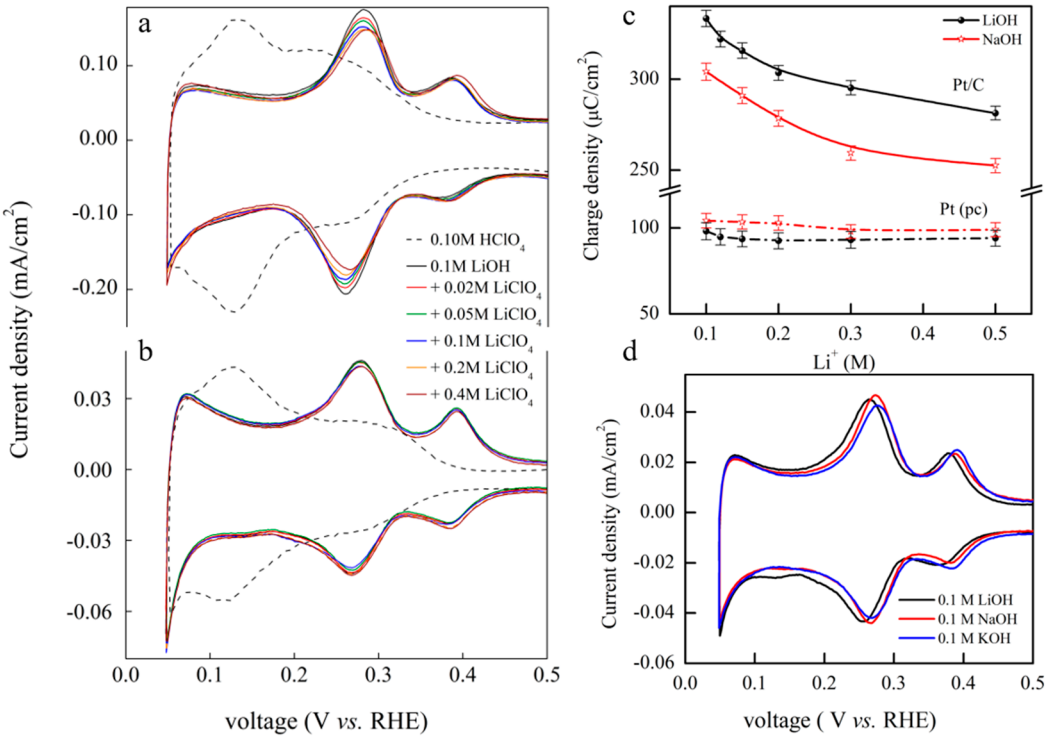

Figure 4. Cyclic voltammograms (CVs) recorded on a Pt/C (a) and Pt polycrystalline electrode (b) in Ar-saturated 0.1 M $HClO_4$ or0.1 M LiOH with varying concentration of $LiClO_4$ with a scan rate of 20 mV/s. (c) Summary of the area (charge) of the anodic H_{UPD} peak of Pt(110) around 0.28 V of the Pt/C and Pt polycrystalline electrode in 0.1 M LiOH with varying concentration of $LiClO_4$ or in 0.1 M NaOH with varying concentration of $NaClO_4$; The error bars derived from variations generated by three measurements. (d) The CVs recorded on the Pt polycrystalline electrode in an Ar-saturated 0.1 M LiOH, NaOH, or KOH electrolyte with a scan rate of 20 mV/s.

conclude that when switching from 0.6 to 0.1 V the major occurrence in the electrolyte of 0.1 M NaOH + 0.4 M $NaClO_4$ is predominately the adsorption of H_{ad} on the fcc site of the Pt/C surface.

On the other hand, the dips of the $\Delta\mu$(0.1 V) spectra of the Pt/C in 0.1 M $HClO_4$ and 0.1 M NaOH are mainly caused by the lower white line intensity in 0.1 V than in 0.6 V, which is observed neither by adding H_2 gas onto Pt nanoclusters[28] nor by adding an H atom onto the Pt_6 cluster model (Figure 3b); meanwhile the shift of the XANES spectra is insignificant. These dips are thus centered around 11 566 eV (Figure 2a,b). The mismatches between the experimental $\Delta\mu$(0.1 V) and the calculated $\Delta\mu_H$ indicate that the H adsorption is not the only occurrence of the Pt/C in 0.1 M $HClO_4$ and 0.1 M NaOH as the potential shifts from 0.6 to 0.1 V.

By far we use the calculated $\Delta\mu$ spectra ($\Delta\mu = \mu(Pt_6{-}A_d) - \mu(Pt_6)$) to compare with the experimental $\Delta\mu$ spectra ($\Delta\mu(U) = \mu(U) - \mu(0.6\ V)$ based on the assumption that the Pt surface at 0.6 V is free of H_{ad}, OH_{ad}, or $H_2O{\downarrow}_{ad}$. However, recent studies suggest the presence of OH_{ad} or $H_2O{\downarrow}_{ad}$ on Pt surfaces within a wide potential range of 0.1−1.0 V in aqueous solutions.[10,14] We therefore examine the possibility of the presence of OH_{ad} and $H_2O{\downarrow}_{ad}$ on Pt surfaces by extending the $\Delta\mu$ analysis to water molecule adsorbates. The Pt−O bond distance is set to be 2.0 Å for OH_{ad} based on experimental FT-EXAFS fits[16] and to be 2.3 Å for $H_2O{\downarrow}_{ad}$ according to a previous study.[29] The calculated XANES of the Pt_6 cluster remains largely unchanged except for a slight increase in the white line intensity when putting the $H_2O{\downarrow}_{ad}$ in atop or bridge site the XANES. On the other hand, its white line intensity drops dramatically when putting the $H_2O{\downarrow}_{ad}$ on the fcc site. Since the dramatic drop of white line intensity is never observed experimentally, the $H_2O{\downarrow}_{ad}$ in the fcc site can be excluded, whereas the $H_2O{\downarrow}_{ad}$ in the atop or bridge site cannot. These calculation results agree with previous DFT calculations that the atop and bridge adsorptions of $H_2O{\downarrow}_{ad}$ are the most stable water adsorption orientations for Pt(100) and Pt(111) facet, respectively.[20] Since the AM^+ effect is absent for the Pt(111) surface[2] and the Pt(111) surface does not bind $H_2O{\downarrow}_{ad}$ within the H_{UPD} potential region,[8] here we focus on the atop adsorption of $H_2O{\downarrow}_{ad}$ only.

We use $Pt_6{-}OH_{atop}$ or $Pt_6{-}H_2O{\downarrow}_{atop}$ as the baseline spectrum to calculate the $\Delta\mu$ spectra, that is, $\Delta\mu_{H-OH} = \mu(Pt_6{-}H_{fcc}) - \mu(Pt_6{-}OH_{atop})$ or $\Delta\mu_{H-H_2O} = \mu(Pt_6{-}H_{fcc}) - \mu(Pt_6{-}H_2O{\downarrow}_{atop})$. The calculated $\Delta\mu_{H-OH}$ or $\Delta\mu_{H-H_2O}$ spectra (Figure 3f) represent the replacement of OH_{ad} or $H_2O{\downarrow}_{ad}$ by H_{ad}, respectively. The $\Delta\mu_H$ that represents the adsorption of hydrogen on a clean Pt surface is codisplayed for comparison. As seen in Figure 3d, while the $\Delta\mu_{H-H_2O}$ has a s-shape feature like the $\Delta\mu_H$, the $\Delta\mu_{H-OH}$ is dramatically different, exhibiting a prominent dip and a wide and flattened plateau. This is essentially because adding one $H_2O{\downarrow}_{ad}$ molecule onto the Pt_6 cluster changes the XANES spectrum slightly, whereas adding OH_{ad} makes a dramatic change because of the profound charge transfer from Pt to the OH_{ad}. These results suggest that the exchange between H_{ad} and OH_{ad} on the surface of Pt/C within the H_{UPD} potential region can be ruled out, whereas the exchange between H_{ad} and $H_2O{\downarrow}_{ad}$ cannot. Moreover, the replacement of the $H_2O{\downarrow}_{ad}$ by H_{ad} at 0.1 V means that fewer Pt−Pt bonds are blocked by $H_2O{\downarrow}_{ad}$ at 0.1 V than at 0.6 V, which accounts for the higher intensity of the Pt−Pt FT-

https://dx.doi.org/10.1021/acscatal.0c02762
ACS Catal. 2020, 10, 11099−11109

EXAFS peaks at 0.1 V (Figure 1). It also accounts for the lower white line intensity of the XANES spectrum at 0.1 V than at 0.6 V observed in 0.1 M $HClO_4$ and 0.1 M NaOH (Figure 2a,b) because the $H_2O{\downarrow}_{ad}$ increases the Pt white line intensity through the charge transfer from Pt to the O (Figure 3d). However, the exchange between H_{ad} and $H_2O{\downarrow}_{ad}$ is not observed in 0.1 M NaOH with 0.4 M $NaClO_4$, for which the $\Delta\mu$ signal is dominated by the adsorption of H_{ad} on a clean Pt surface. This result suggests that the Na^+ suppresses the exchange between H_{ad} and $H_2O{\downarrow}_{ad}$ on Pt surfaces in alkaline solutions.

Collectively, the in situ XAS results discard specific adsorption of Na^+ on Pt surfaces and the exchange between H_{ad} and OH_{ad} within the H_{UPD} potential region in alkaline solutions and alternatively suggest the exchange between H_{ad} and $H_2O{\downarrow}_{ad}$. These results therefore pose questions on the previous argument that explains the sharp H_{UPD} peaks of stepped Pt surfaces and their non-Nernstian pH shift based on specific adsorption of AM^+ and OH_{ad}.[8,13] In an attempt to consolidate alternative explanations on the basis of the in situ XAS results, we explore the AM^+ effects on the H_{UPD} peaks as well as the HER/HOR kinetic of Pt surfaces electrochemically. The HER/HOR is chosen here not only because they are the most fundamentally important electrochemical reactions but also because the HER/HOR rates of Pt are intimately related to the H_{UPD} peak position.[30]

2.2. Electrochemical Studies. We first evaluate the AM^+ effects on the CV features of Pt surfaces including the same Pt/C subject to XAS measurements and a Pt polycrystalline electrode in both acidic and alkaline solutions. Detailed rotating disk electrode (RDE) measurements are provided in the Experimental Methods.

The CVs of Pt/C and Pt polycrystalline electrodes in 0.1 M $HClO_4$ or 0.1 M LiOH with varying concentrations of $LiClO_4$ are displayed in Figure 4a,b, respectively. The integral area of the anodic H_{UPD} peak (~0.28 V) of the Pt(110) facet in the Pt/C gradually decrease around 20% as the Li^+ or Na^+ (Figure S3) concentration increases from 0.1 to 0.5 M; meanwhile, those of the Pt polycrystalline electrode remain nearly unchanged (Figure 4c). These different results indicate that the poisoning caused by the impurities in the highly purified $LiClO_4$ (99.99%) and $NaClO_4$ (99.99%), if there is any, has minimal impacts on the reduction of the Pt(110) peak intensity of the Pt/C. We therefore relate the reduction of the Pt(110) peak intensity of the Pt/C primarily to the increased AM^+ concentration. In other words, the AM^+ suppresses the occurrence that generates the sharp H_{UPD} peaks of Pt(110). In parallel to this electrochemical observation, the XAS results suggest that the AM^+ suppresses the exchange between H_{ad} and $H_2O{\downarrow}_{ad}$ on Pt surfaces, which leads to the deduction that the sharp H_{UPD} peak of Pt(110) originated by the exchange between H_{ad} and the $H_2O{\downarrow}_{ad}$. The sharpness feature of the H_{UPD} peak of Pt(110) can be ascribed to the attractive interaction between H_{ad} and $H_2O{\downarrow}_{ad}$, following the previous one attributing the sharp H_{UPD} peaks of stepped Pt surfaces to the exchange between H_{ad} and OH_{ad}.[31] In acidic solutions, this reaction can be expressed as

$$Pt{-}H_{ad} + H_2O{\downarrow} \leftrightarrow Pt{-}H_2O{\downarrow}_{ad} + H^+ + e^- \quad (1)$$

The $H_2O{\downarrow}$ represents the water molecule with the O pointing toward the Pt surface leading to a direct Pt−O bond. The specific adsorption mode of $H_2O{\downarrow}_{ad}$ may be either atop or bridge as suggested by $\Delta\mu$ (Figure 3f). This reaction also occurs in alkaline solutions upon the anodic sweep, followed by H^+ migrating into the electrolyte reacting with OH^- forming water there:

$$H^+ + OH^- \leftrightarrow H_2O \quad (2)$$

and the sum of the Reaction 1 and 2 gives

$$Pt{-}H_{ad} + OH^- \leftrightarrow Pt{-}H_2O{\downarrow}_{ad} + e^- \quad (3)$$

The backward direction of Reaction 3 represents the hydrogen adsorption in alkaline solutions during the cathodic sweep. Therefore, the exchange of the H_{ad} and $H_2O{\downarrow}_{ad}$ on stepped Pt surfaces is a reversible process in acid (Reaction 1) but is not in alkaline because while $H_2O{\downarrow}_{ad}$ dissociation generates OH^- (Reaction 3, backward direction), it is the $H_2O{\downarrow}$ rather than OH^- that removes H_{ad} (Reaction 1, forward direction). This argument agrees with the experimental observations by Tang et al.[9] that the H_{UPD} peaks of Pt(110) are reversible in acid but not in alkaline.

By this hypothesis, the AM^+ suppresses the exchange of H_{ad} and $H_2O{\downarrow}_{ad}$ by reducing the abundance of $H_2O{\downarrow}_{ad}$ by means of converting free water molecules to water molecules coordinated to AM^+ (coordinating water) ($[(H_2O)_x{-}AM]^+$).[32] As a result, more Pt sites are underneath the $[(H_2O)_x{-}AM]^+$ inaccessible by $H_2O{\downarrow}$ and thus undergo the "regular" H adsorption/desorption process involving $H_2O{\uparrow}$. The $H_2O{\uparrow}$ represents the water molecule with the H facing toward the Pt surface. It can be either free water or coordinating water.

No significant shifts of the H_{UPD} peak position are observed for both Pt polycrystalline electrode and Pt/C as the Li^+ concentration increases to 0.5 M (0.1 M LiOH + 0.4 M $LiClO_4$). This result is consistent with the recent observation by Xu et al.[14] that the H_{UPD} peaks of the single crystals of Pt(110) and Pt(100) do not exhibit a discernible shift in the alkaline solution of 0.1 M KOH plus varying concentrations of $KClO_4$. In a comprehensive study, Koper et al.[13] showed that the AM^+-induced shift of the H_{UPD} peak position of Pt(110) is pH dependent. The H_{UPD} peak position of Pt(110) does not shift with AM^+ in the acidic solution with the pH of 1−2. It shifts anodically around 30 mV as the AM^+ concentration increases to 0.1 M in the acidic solution with the pH of 3. However, the shift becomes insignificant in the alkaline solution with the pH of 11,[13] which is consistent with our and Xu et al.'s[14] results. Meanwhile, the H_{UPD} peak position of Pt(110) shift markedly when changing the identity of the AM^+ in the aqueous solutions within a wide pH range of 3−13.[13] The same phenomenon is also observed by us in the alkaline solution with a pH value of 13 (Figure 4d). These results together conclude that the AM^+ does affect the H_{UPD} peak position of Pt(110), despite the debate on the adsorption mode of AM^+. Koper et al.[13] ascribed the shift of the H_{UPD} peak of stepped Pt surfaces with pH exclusively to the weakening of the $Pt{-}OH_{ad}$ bond by the specifically adsorbed AM^+. Since in situ XAS identifies neither specifically adsorbed AM^+ nor OH_{ad} but rather $H_2O{\downarrow}_{ad}$, we alternatively propose that the AM^+-induced shift of the H_{UPD} peak of stepped Pt surfaces originates from the weakening of the $Pt{-}H_2O{\downarrow}_{ad}$ bond by the noncovalent interaction with $[(H_2O)_x{-}AM]^+$, which leads to the sandwich structure of $Pt{-}H_2O{\downarrow}_{ad}{\cdots}[(H_2O)_x{-}AM]^+$ across the interface.

By taking the $Pt{-}H_2O{\downarrow}_{ad}{\cdots}[(H_2O)_x{-}AM]^+$ into consideration, the Reaction 1 can be rewritten as

https://dx.doi.org/10.1021/acscatal.0c02762
ACS Catal. 2020, 10, 11099−11109

$$Pt{-}H_{ad} + H_2O{\downarrow}{+}[(H_2O)_x{-}AM]^+ \leftrightarrow Pt{-}H_2O{\downarrow}_{ad}\cdots[(H_2O)_x{-}AM]^+ + H^+ + e^- \quad (4)$$

and the Reaction 3 can be rewritten as

$$Pt{-}H_2O{\downarrow}_{ad}\cdots[(H_2O)_x - AM]^+ + e^- \rightarrow Pt{-}H_{ad} + OH^- - [(H_2O)_x{-}AM]^+ \quad (5)$$

Reactions 4 and 5 represent the exchange between the H_{ad} and $H_2O{\downarrow}_{ad}\cdots[(H_2O)_x{-}AM]^+$ on undercoordinated Pt sites and are responsible for the anodic and cathodic H_{UPD} peaks of stepped Pt surfaces, respectively (Scheme 1). The stronger the

Scheme 1. Schematic Illustration of the Exchange between H_{ad} and $H_2O{\downarrow}_{ad}\cdots[(H_2O)_x{-}AM]^+$ as the Causes of the Sharp H_{UPD} Peaks of Stepped Pt Surfaces in Alkaline Solutions

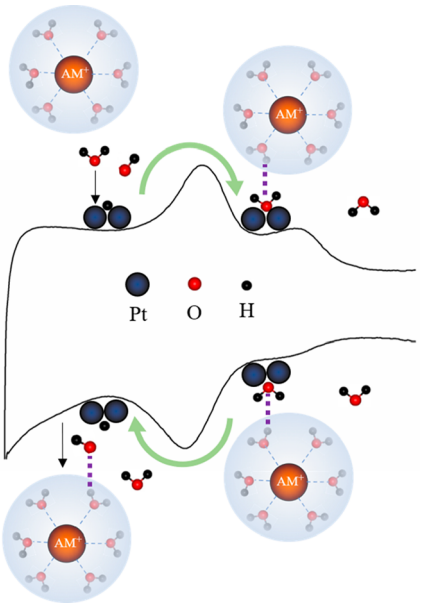

noncovalent $H_2O{\downarrow}_{ad}\cdots[(H_2O)_x{-}AM]^+$ bond, the weaker the $Pt{-}H_2O{\downarrow}_{ad}$ bond, and the more positive the corresponding H_{UPD} peak. Among various AM^+ species, Li^+ is the hardest Lewis acid and therefore the $[(H_2O)_x\text{-}Li]^+$ has the weakest bond with $H_2O{\downarrow}_{ad}$ that is a soft Lewis base as per the HSAB theory. Li^+ thus weakens the $Pt{-}H_2O{\downarrow}_{ad}$ bond the least, and correspondingly, the H_{UPD} peak of Pt surfaces is located in the lowest potential vs. RHE. This argument agrees with the previous one that AM^+ weakens the $Pt{-}OH_{ad}$ bond and Li^+ weakens the least,[13] despite the different oxygen adsorbate ($H_2O{\downarrow}_{ad}$ vs. OH_{ad}) and adsorption mode of AM^+ (nonspecific vs. specific). It however conflicts the argument by Markovic et al.[2] that the noncovalent bond within $OH_{ad}\cdots[(H_2O)_x{-}AM]^+$ is the strongest with Li^+, despite the agreement on the nonspecific adsorption of AM^+.

While the AM^+ affects the $Pt{-}H_2O{\downarrow}_{ad}$ bond strength from the $H_2O{\downarrow}_{ad}$ side, the pH affects the $Pt{-}H_2O{\downarrow}_{ad}$ bond strength from the Pt side. By using Quantum Mechanics Molecular Dynamics simulation, Goddard et al.[23] recently showed that increasing pH makes the stepped Pt surface repel the $H_2O{\downarrow}_{ad}$, thereby weakening the $Pt{-}H_2O{\downarrow}_{ad}$ bond. This result consistently relates to the previous argument that as the pH increases, the potential of zero free charge shifts positively toward higher potentials,[33] which in turn makes the Pt surface more negatively charged and in turn repels the negatively charged O in the $H_2O{\downarrow}_{ad}$. Therefore, the non-Nernstian pH shift of the H_{UPD} peaks of stepped Pt surfaces originates from the weakening the $Pt{-}H_2O{\downarrow}_{ad}$ bond by pH as well as AM^+. Another possible contribution from the partial oxidation of $H_2O{\downarrow}_{ad}$ cannot be excluded here.[34,35] This notion provides a reasonable explanation of previous observations[13] that changing either pH or AM^+ concentration/identity can shift the H_{UPD} peaks of stepped Pt surfaces.

Our new hypothesis can also account for the profound effects of AM^+ on the HER/HOR kinetics of stepped Pt surfaces in alkaline solutions. The HER/HOR rates of the Pt/C and Pt polycrystalline electrode with increasing Li^+ concentration in the 0.1 M LiOH solution are assessed in a RDE. The polarization curves displayed in Figure 5 are IR-corrected to account for the reduction of the electrolyte impedance with increasing Li^+ concentration (Table S2). As the Li^+ concentration gradually increases to 0.3 M, the HER current density of Pt/C increases first and then drops, whereas the HOR current density drops monotonously (Figure 5a). Additionally, both the HER and HOR kinetic current density of the Pt polycrystalline electrode drop monotonously with increasing Li^+ concentration (Figure 5d). For both cases, the same trends are also observed on the exchange current density (Figure 5b and 5d, inset), and the kinetic current densities in the Tafel plots (Figure 5c,e) that are normalized by the Li^+ concentration induced variation of the HOR limiting current density. The HOR limiting current density for both cases drops slightly with increasing concentration of Li^+ (Figure 5a inset and Figure 5d), which is primarily caused by the increasing kinematic viscosity, decreasing H_2 diffusion coefficient and solubility of the electrolyte.[36] To quantitatively summarize the HER/HOR current density trends of the Pt/C and Pt polycrystalline as a function of Li^+ concentration, the current densities at ±0.06 V acquired from the Tafel plots are displayed in Figure 5f. As seen, the HER/HOR rates of the Pt polycrystalline electrode drop simultaneously with increasing Li^+ concentration. The HOR rate of the Pt/C also drops with increasing Li^+ concentration, whereas the HER rate increases until the Li^+ reaches 0.2 M, and then drops (Figure 5f).

The increasing HER rate of Pt/C with increasing Li^+ concentration up to 0.2 M was previously reported by us[5] and ascribed to the Li^+-facilitated removal of the OH_{ad} generated from water:

$$Pt{-}OH_{ad}\cdots[(H_2O)_x{-}AM]^+ + e^- \leftrightarrow Pt + OH^-\cdots[(H_2O)_x{-}AM]^+ \quad (6)$$

Wherein $OH_{ad}\cdots[(H_2O)_x{-}AM]^+$ is generated from dissociation of the $H_2O{\downarrow}_{ad}$ in $H_2O{\downarrow}_{ad}\cdots[(H_2O)_x{-}AM]^+$. We previously proposed that Reaction 6 is the rate-determining step (rds) for the HER of Pt in alkaline as part of the Volmer.[5] Reaction 6 is kinetically faster than the counterpart one without the coordinating water: $Pt{-}OH_{ad}\cdots(H_2O)_x + e^- \leftrightarrow Pt + OH^-\cdots(H_2O)_x$ because the coordinating water facilitates OH_{ad} removal as per the HSAB theory.[5] Therefore, enriching the content of $Pt{-}OH_{ad}\cdots[(H_2O)_x{-}AM]^+$ or essentially the $Pt{-}H_2O{\downarrow}_{ad}\cdots[(H_2O)_x{-}AM]^+$) improves the HER kinetics. The content of $Pt{-}H_2O{\downarrow}_{ad}\cdots[(H_2O)_x{-}AM]^+$ is limited by the content of either undercoordinated Pt sites or AM^+ depending on which one saturates. As for the case of Pt/C, the HER rate increases as the content of the $Pt{-}OH_{ad}\cdots[(H_2O)_x\text{-}Li]^+$ increases until the undercoordinated Pt sites saturate with

https://dx.doi.org/10.1021/acscatal.0c02762
ACS Catal. 2020, 10, 11099−11109

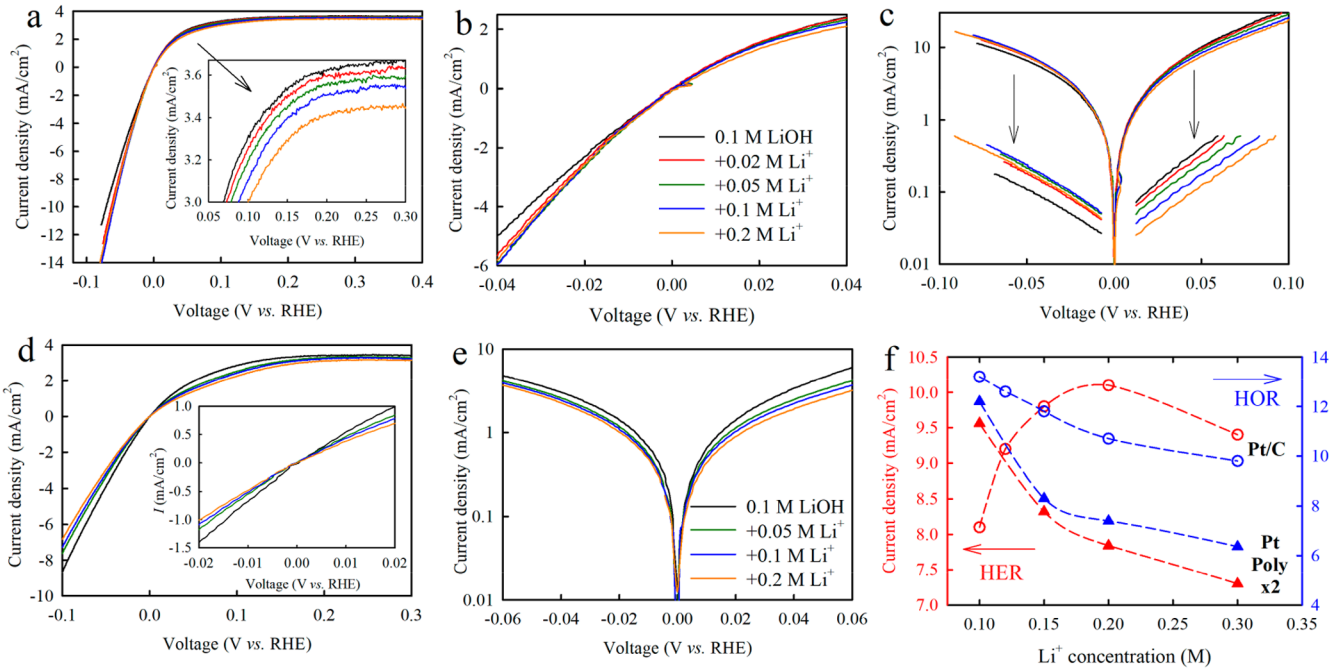

Figure 5. (a) The HER/HOR polarization curves of Pt/C in 0.1 M LiOH plus increasing concentration of $LiClO_4$. The zoomed region of the HOR limiting current is present in the inset. (b) The exchange current region of the HER/HOR curves displayed in (a). (c) The Tafel plots of the HER/HOR curves displayed in (a), with zoomed in regions to show the trend. (d) The HER/HOR polarization curves of the Pt polycrystalline electrode in 0.1 M LiOH plus increasing concentration of $LiClO_4$. The zoomed region of the exchange current density region is present in the inset. (e). The Tafel plots of the HER/HOR curves displayed in (d). (f) The HER/HOR current densities acquired at ±0.06 V in (c) and (e) as a function of Li^+ concentration. The current densities of the Pt polycrystalline electrode are scaled by a factor of 2 to ease the display.

~0.2 M Li^+. As the Li^+ concentration increases further, the content of the $H_2O{\downarrow}_{ad}\cdots[(H_2O)_x{-}AM]^+$) starts to decrease because the content of the free water $H_2O{\downarrow}$ in the electrolyte decreases, resulting in the decrease of the content of Pt–$H_2O{\downarrow}_{ad}$ (eq 4) and in turn the decrease of the HER rate of Pt/C. We previously showed that the OH_{ad} anchor sites of Pt/C can be increased by surface doping Ni, and consequently, the HER rate of the Pt–Ni/C system continuously increases as the Li^+ concentration increases to 0.3 M.[5] Additionally, further increasing Li^+ in 0.1 M LiOH only reduces the HER rate of the Pt polycrystalline electrode (Figure 5f). This is because the undercoordinated Pt sites of the Pt polycrystalline electrode are much less than those in Pt/C as reflected by the much lower roughness factor of Pt polycrystalline electrode compared with that of Pt/C,[29] which is essentially because the number of surface undercoordinated sites decreases with increasing Pt particle size.[37] As a result, the undercoordinated Pt sites of Pt polycrystalline electrode are already saturated in 0.1 M LiOH. Moreover, the saturation of undercoordinated Pt sites of the Pt polycrystalline electrode in 0.1 M LiOH also accounts for the observation that its H_{UPD} peak intensity does not drop with increasing Li^+ concentration (Figure 4c) like Pt/C.

The rds of the HOR of undercoordinated Pt surfaces in alkaline solutions is the Reaction 4 that is also part of the Volmer step. Since the presence of AM^+ weakens the Pt–$H_2O{\downarrow}_{ad}$ bond thereby delaying the H_{ad} oxidation, increasing AM^+ concentration only decreases the HOR rate of undercoordinated Pt surfaces, as observed on the Pt/C and Pt polycrystalline electrode. Furthermore, since the Li^+ weakens the Pt–$H_2O{\downarrow}_{ad}$ bond the least among AM^+, the HOR rate of stepped Pt surfaces in LiOH is the highest.[5] In a recent study, we propose that the surface Ru promotes the HOR of Pt in alkaline solutions by hosting $H_2O{\downarrow}_{ad}$ at low potentials without dissociating it and the $H_2O{\downarrow}_{ad}$ removes the H_{ad} on the nearby Pt via L-H mechanism,[38] which is consistent with the proposed notion here. By this new notion, the AM^+ effects on the CV features of Pt surfaces and the HER/HOR kinetics are unified by the noncovalent interactions between hydrated AM^+ and Pt surfaces with oxygen adsorbates. Because the sharp H_{UPD} peak of undercoordinated Pt surfaces arises from the exchange between H_{ad} by $H_2O{\downarrow}_{ad}$ (Scheme 1), which are the rds of the HER/HOR of Pt, the HER/HOR rate of Pt in high pH solutions closely correlates with the H_{UPD} peak position.

This study focuses exclusively on the adsorption mode of AM^+ and the catalytic effects on the Pt electrode in alkaline solutions, providing insights into fundamental alkaline electrochemistry. It can be extended to organic cations on other metal electrodes in other interfacial environments (aqueous and nonaqueous) for both fundamental and practical applications. For instance, recent studies showed that quaternary ammonium cations, which are used in polymer ionomers and membranes to provide anionic conductivity, adsorb specifically on a Pt electrode and have profound effects on the HER/HOR activity of the Pt electrode.[39,40] Such insights will help to guide the design of catalysts, ionomer, and membrane for alkaline fuel cells.

3. CONCLUSIONS

In summary, the in situ XAS experiments coupled with FEFF6 calculations rule out specific adsorption of AM^+ and OH_{ad} but not $H_2O{\downarrow}_{ad}$ on the surface of Pt/C within the H_{UPD} potential region in alkaline solutions with the AM^+ concentration up to 0.5 M. Meanwhile, electrochemical measurements highlight the

https://dx.doi.org/10.1021/acscatal.0c02762
ACS Catal. 2020, 10, 11099−11109

profound and comprehensive effects of AM^+ on the H_{UPD} peaks and HER/HOR activity of Pt surfaces in alkaline solutions. We propose the presence of the sandwich structure of $Pt-H_2O{\downarrow}_{ad}\cdots[(H_2O)_x-AM]^+$ across the interface in which the $H_2O{\downarrow}_{ad}$ is specifically adsorbed on undercoordinated Pt surfaces and interacts with the $[(H_2O)_x-AM]^+$ via non-covalent interactions, and underscore the $Pt-H_2O{\downarrow}_{ad}\cdots[(H_2O)_x-AM]^+$ as the key species determining the catalytic properties of undercoordinated Pt surfaces in aqueous solutions. Specifically, the sharp H_{UPD} peaks of stepped Pt surfaces arise from the exchange between H_{ad} and $H_2O{\downarrow}_{ad}\cdots[(H_2O)_x-AM]^+$, and their non-Nernstian pH shift is caused by the weakening of the $Pt-H_2O{\downarrow}_{ad}$ bond by the $[(H_2O)_x-AM]^+$ as well as by the pH increase. The AM^+ is detrimental to the HOR of Pt since the $[(H_2O)_x-AM]^+$ weakens the $Pt-H_2O{\downarrow}_{ad}$, thereby delaying the oxidation of H_{ad}. On the other hand, the AM^+ can be beneficial to the HER of Pt by facilitating the removal of the OH_{ad} in the form of $OH_{ad}\cdots[(H_2O)_x-AM]^+$ that is formed upon the dissociation of $H_2O{\downarrow}_{ad}$. In a broad context, the $H_2O{\downarrow}_{ad}\cdots[(H_2O)_x-AM]^+$ is believed to be widely present in the interface in aqueous solutions dictating the catalytic activity toward many reactions such as oxygen reduction/evolution reactions on catalysts with affinities toward interfacial water.

4. EXPERIMENTAL METHODS

Chemicals. Carbon supported platinum nanoparticles (Pt/C, 47.2 wt.%) were purchased from Tanaka Kikinzoku Kogyo. Nickel(II) perchlorate ($Ni(ClO_4)_2$, 98%), lithium perchlorate ($LiClO_4$, 99.99%), lithium hydroxide (LiOH, > 98%), sodium hydroxide (NaOH, > 98%), potassium hydroxide (KOH, 99.99%), and perchloric acid ($HClO_4$, 70%, PPT grade) were all purchased from Sigma-Aldrich. All aqueous solutions were prepared using deionized (DI) water (18.2 MΩ·cm) obtained from an ultrapure purification system (Aqua Solutions).

Electrode Preparation. The preparation of the thin-film electrodes of Pt/C and Pt polycrystalline electrode was followed our previous study.[5] The average particle size of the Pt/C determined by transmission electron microscopy was 2.0 ± 0.4 nm based on around 200 particle counts. 2−3 mg catalyst powders were added into the mixture of 1 mL of DI water (18.2 MΩ·cm), 1 mL of isopropyl alcohol, and 5 μL of Nafion (5%). The aqueous suspensions were sonicated for 45 min with an ice bath, and deposited onto the electrode surface with a rotation rate of 500−700 rpm, and dried in air at room temperature for 20 min to achieve a Pt loading of ~10ug·cm^{-2}. Prior to the electrodeposition, the glass carbon electrode embedded in PTFE or the Pt polycrystalline electrode was polished mechanically by 0.5, 0.3, and 0.05 μm alumina powder and then sonicated in sequence for 5 min in DI water and ethanol.

Electrochemical Measurements. All the electrochemical experiments were conducted using a three-electrode cell system. The working electrode was a glassy carbon rotating disk electrode (RDE) from Pine Instruments, and the glassy carbon geometry area is 0.2463 cm^2; or a Pt polycrystalline from Pine Instruments with the geometry area of 0.2124 cm^2. Pt wire and Ag/AgCl (1 M Cl^-) were used as the counter and reference electrodes respectively. All potentials reported in this paper are referenced to the reversible hydrogen electrode (RHE), calibrated in the same electrolyte by measuring the potential of the HOR/HER currents at zero corresponding to 0 V versus RHE (V_{RHE}).

Prior to the RDE testing, the RDE electrode with the catalyst was cycled with a rotation rate of 1600 rpm in an Ar-saturated 0.1 M $HClO_4$ electrolyte with a scan rate of 500 mV·s^{-1} between the potential range of 0.05−1.2 V for 100 cycles.[41] This harsh acid conditioning process sufficiently clears and stabilizes the Pt surfaces and makes the subsequent RDE measurements repeatable. Then the electrode was immersed in a fresh Ar-purged 0.1 M $HClO_4$ electrolyte for the CV measurements with a scan rate of 20 mV·s^{-1}. Afterward, the same electrode was immersed in a fresh Ar-purged 0.1 M NaOH or LiOH electrolyte for CV measurements. The CVs of both Pt/C and Pt polycrystalline electrodes reached stable status after five scans. Then varying amounts of high purity of solid $LiClO_4$ or $NaClO_4$ (Sigma-Aldrich, > 99.9%) were dissolved in 0.1 M LiOH or NaOH, and the solution was added into the 0.1 M LiOH or NaOH electrolyte to reach the desired AM^+ concentration. The H_{UPD} charge was derived with identical parameters in the alkaline electrolyte with increasing concentration of AM^+.

HER/HOR tests were conducted in a H_2-saturated alkaline electrolyte at room temperature with a scan rate of 10 mVs^{-1} and a potential range of −1.2−0 V vs Ag/AgCl with a rotation rate of 2500 rpm. The CVs were recorded in Ar-saturated LiOH between 0.05 and 1.1 V_{RHE} at a scan rate of 20 mV s^{-1} after it reached the steady state. The HOR kinetic current densities (i_k) were obtained from correcting the polarization curves by the hydrogen mass transport in the HOR branch using the Koutecky−Levich equation. All the electrochemical active surface area (ECSA) was determined by integrating hydrogen adsorption charge on CV curves by assuming a value of 210 μC·cm^{-2} for the adsorption of one hydrogen monolayer unless mentioned otherwise. Double-layer correction was applied.

Impedance Measurements. The impedance spectra were measured with frequencies from 10^5 to 0.1 Hz with amplitude of 10 mV by Autolab. Equivalent circuits were fitted to the data with Zview software. The solution resistances measured at room temperature as a function of Li^+ concentration, and applied potentials were systematically evaluated.

Adding $LiClO_4$. $LiClO_4$ was dissolved into 0.1 M LiOH resulting in a concentration of 1 M $LiClO_4$ solution. A selected amount of solution was then added into the 0.1 M LiOH electrolyte (~80 mL) to vary the Li^+ concentration in the electrolyte in a controlled manner.

In Situ XAS Data Collection and Analysis. The preparation method of the XAS electrodes can be referred to our previous work.[24] The final Pt geometric loadings were chosen to give 0.3 transmission spectra edge heights at the Pt L_3 edge. The XAS experiments were conducted at room temperature in a previously described flow half−cell[42] in which continuously Ar-purged 0.1 M KOH or 0.1 M $HClO_4$ was circulated. The voltage cycling limits were 0 to 0.6 V_{RHE}. The data at the Pt edge of the Pt/C were collected in the transmission mode at the beamlines QAS 7-BM and ISS 8-ID of the National Synchrotron Light Source (NSLS) II, Brookhaven National Laboratory (BNL). Typical experimental procedures were utilized with details provided in our previous work.[24]

The XAS data were processed and fitted using the Ifeffit-based Athena[43] and Artemis[44] programs. Scans were calibrated, aligned, and normalized with background removed using the IFEFFIT suite.[45] The χ(R) was modeled using single scattering paths calculated by FEFF6.[46] The $\Delta\mu$ analysis technique has

https://dx.doi.org/10.1021/acscatal.0c02762
ACS Catal. 2020, 10, 11099−11109

been described in great detail elsewhere.[16,17,24,47] Briefly, difference spectra were calculated using the equation:

$$\Delta\mu(\mathrm{U}) = \mu(\mathrm{U}) - \mu(0.6\mathrm{V})$$

where $\mu(\mathrm{U})$ is the absorption coefficient of the sample at a potential of interest and $\mu(0.6\ \mathrm{V})$ is the reference signal at 0.6 V, which is considered the clean double layer region for platinum (i.e., free of any adsorbed H, O(H), or oxygen adsorbates).

■ ASSOCIATED CONTENT

Supporting Information

The Supporting Information is available free of charge at https://pubs.acs.org/doi/10.1021/acscatal.0c02762.

Sample preparation, EXAFS fits, full set of XANES spectra, and electrochemical studies on the Pt/C in 0.1 M NaOH with additional varying concentration of $NaClO_4$, impedance measurements as a function of Li^+ concentrations (PDF)

■ AUTHOR INFORMATION

Corresponding Author

Qingying Jia − *Department of Chemistry and Chemical Biology, Northeastern University, Boston, Massachusetts 02115, United States;* orcid.org/0000-0002-4005-8894; Email: q.jia@northeastern.edu

Authors

Li Jiao − *Department of Chemical Engineering, Northeastern University, Boston, Massachusetts 02115, United States*

Ershuai Liu − *Department of Chemistry and Chemical Biology, Northeastern University, Boston, Massachusetts 02115, United States*

Sanjeev Mukerjee − *Department of Chemistry and Chemical Biology, Northeastern University, Boston, Massachusetts 02115, United States*

Complete contact information is available at: https://pubs.acs.org/10.1021/acscatal.0c02762

Author Contributions

Q.J. conceived the project. Q.J. conceived and designed the in situ XAS experiments and electrochemical experiments. L.J. conducted the electrochemical experiments and analyzed the data. E.L. conducted some of the electrochemical experiments. Q.J. and S.M. supervised and advised the electrochemical experiments and data analysis. L.J., E.L., and Q.J. conducted the in situ XAS experiments. Q.J. analyzed the XAS data. Q.J. derived the new notion. Q.J. and L.J. wrote the manuscript.

Notes

The authors declare no competing financial interest.

■ ACKNOWLEDGMENTS

This work was supported by the Office of Naval Research (ONR) under award number N00014-18-1-2155, as well as by the U.S. Department of Energy under award numbers DE-EE0008416. The authors declare no competing financial interests. This research used beamline 7-BM (QAS) and 8-ID (ISS) of the National Synchrotron Light Source II, a U.S. Department of Energy (DOE) Office of Science User Facility operated for the DOE Office of Science by Brookhaven National Laboratory under Contract No. DE-SC0012704.

■ REFERENCES

(1) Teliska, M.; Murthi, V. S.; Mukerjee, S.; Ramaker, D. E. Site-Specific vs Specific Adsorption of Anions on Pt and Pt-Based Alloys. *J. Phys. Chem. C* **2007**, *111*, 9267−9274.

(2) Strmcnik, D.; Kodama, K.; van der Vliet, D.; Greeley, J.; Stamenkovic, V. R.; Marković, N. M. The Role of Non-Covalent Interactions in Electrocatalytic Fuel-Cell Reactions on Platinum. *Nat. Chem.* **2009**, *1*, 466.

(3) Danilovic, N.; Subbaraman, R.; Strmcnik, D.; Paulikas, A. P.; Myers, D.; Stamenkovic, V. R.; Markovic, N. M. The Effect of Noncovalent Interactions on the HOR, ORR, and HER on Ru, Ir, And $Ru_{0.50}Ir_{0.50}$ Metal Surfaces in Alkaline Environments. *Electrocatalysis* **2012**, *3*, 221−229.

(4) Subbaraman, R.; Tripkovic, D.; Strmcnik, D.; Chang, K.-C.; Uchimura, M.; Paulikas, A. P.; Stamenkovic, V.; Markovic, N. M. Enhancing Hydrogen Evolution Activity in Water Splitting by Tailoring Li^+-$Ni(OH)_2$-Pt Interfaces. *Science* **2011**, *334*, 1256−1260.

(5) Liu, E.; Li, J.; Jiao, L.; Doan, H. T. T.; Liu, Z.; Zhao, Z.; Huang, Y.; Abraham, K. M.; Mukerjee, S.; Jia, Q. Unifying the Hydrogen Evolution and Oxidation Reactions Kinetics in Base by Identifying the Catalytic Roles of Hydroxyl-Water-Cation Adducts. *J. Am. Chem. Soc.* **2019**, *141*, 3232−3239.

(6) Giles, S. A.; Wilson, J. C.; Nash, J.; Xu, B.; Vlachos, D. G.; Yan, Y. Recent Advances in Understanding the pH Dependence of the Hydrogen Oxidation and Evolution Reactions. *J. Catal.* **2018**, *367*, 328−331.

(7) Janik, M. J.; McCrum, I. T.; Koper, M. T. On the Presence of Surface Bound Hydroxyl Species on Polycrystalline Pt Electrodes in the "Hydrogen Potential Region"(0−0.4 V_{RHE}). *J. Catal.* **2018**, *367*, 332−337.

(8) McCrum, I. T.; Janik, M. J. pH and Alkali Cation Effects on the Pt Cyclic Voltammogram Explained Using Density Functional Theory. *J. Phys. Chem. C* **2016**, *120*, 457−471.

(9) Intikhab, S.; Snyder, J. D.; Tang, M. H. Adsorbed Hydroxide Does Not Participate in the Volmer Step of Alkaline Hydrogen Electrocatalysis. *ACS Catal.* **2017**, *7*, 8314−8319.

(10) Tanaka, H.; Sugawara, S.; Shinohara, K.; Ueno, T.; Suzuki, S.; Hoshi, N.; Nakamura, M. Infrared Reflection Absorption Spectroscopy of OH Adsorption on the Low Index Planes of Pt. *Electrocatalysis* **2015**, *6*, 295−299.

(11) Zheng, J.; Sheng, W.; Zhuang, Z.; Xu, B.; Yan, Y. Universal Dependence of Hydrogen Oxidation and Evolution Reaction Activity of Platinum-Group Metals on pH and Hydrogen Binding Energy. *Sci. Adv.* **2016**, *2*, e1501602.

(12) García, G. Correlation between CO Oxidation and H Adsorption/Desorption on Pt Surfaces in a Wide pH Range: The Role of Alkali Cations. *ChemElectroChem* **2017**, *4*, 459−462.

(13) Chen, X.; McCrum, I. T.; Schwarz, K. A.; Janik, M. J.; Koper, M. T. M. Co-adsorption of Cations as the Cause of the Apparent pH Dependence of Hydrogen Adsorption on a Stepped Platinum Single-Crystal Electrode. *Angew. Chem., Int. Ed.* **2017**, *56*, 15025−15029.

(14) Yang, X.; Nash, J.; Oliveira, N.; Yan, Y.; Xu, B. Understanding the pH Dependence of Underpotential Deposited Hydrogen on Platinum. *Angew. Chem., Int. Ed.* **2019**, *58*, 17718−17723.

(15) Arruda, T. M.; Shyam, B.; Ziegelbauer, J. M.; Mukerjee, S.; Ramaker, D. E. Investigation into the Competitive and Site-Specific Nature of Anion Adsorption on Pt Using In Situ X-ray Absorption Spectroscopy. *J. Phys. Chem. C* **2008**, *112*, 18087−18097.

(16) Teliska, M.; O'Grady, W. E.; Ramaker, D. E. Determination of O and OH Adsorption Sites and Coverage in Situ on Pt Electrodes from Pt L_{23} X-ray Absorption Spectroscopy. *J. Phys. Chem. B* **2005**, *109*, 8076−8084.

(17) Teliska, M.; O'Grady, W. E.; Ramaker, D. E. Determination of H Adsorption Sites on Pt/C Electrodes in HClO4 from Pt L_{23} X-ray Absorption Spectroscopy. *J. Phys. Chem. B* **2004**, *108*, 2333−2344.

(18) Rehr, J. J.; Kas, J. J.; Prange, M. P.; Sorini, A. P.; Takimoto, Y.; Vila, F. Ab initio theory and calculations of X-ray spectra. *C. R. Phys.* **2009**, *10*, 548−559.

(19) Zadick, A.; Dubau, L.; Sergent, N.; Berthomé, G.; Chatenet, M. Huge Instability of Pt/C Catalysts in Alkaline Medium. *ACS Catal.* **2015**, *5*, 4819−4824.
(20) Seong, S.; Anderson, A. B. Water Dissociation on Pt(111) and (100) Anodes: Molecular Orbital Theory. *J. Phys. Chem.* **1996**, *100*, 11744−11747.
(21) Rehr, J. J.; Kas, J. J.; Vila, F. D.; Prange, M. P.; Jorissen, K. Parameter-Free Calculations of X-Ray Spectra with FEFF9. *Phys. Chem. Chem. Phys.* **2010**, *12*, 5503−5513.
(22) Janin, E.; von Schenck, H.; Göthelid, M.; Karlsson, U. O.; Svensson, M. Bridge-Bonded Atomic Oxygen on Pt(110). *Phys. Rev. B: Condens. Matter Mater. Phys.* **2000**, *61*, 13144−13149.
(23) Cheng, T.; Wang, L.; Merinov, B. V.; Goddard, W. A. Explanation of Dramatic pH-Dependence of Hydrogen Binding on Noble Metal Electrode: Greatly Weakened Water Adsorption at High pH. *J. Am. Chem. Soc.* **2018**, *140*, 7787−7790.
(24) Jia, Q.; Liang, W.; Bates, M. K.; Mani, P.; Lee, W.; Mukerjee, S. Activity Descriptor Identification for Oxygen Reduction on Platinum-Based Bimetallic Nanoparticles: In Situ Observation of the Linear Composition−Strain−Activity Relationship. *ACS Nano* **2015**, *9*, 387−400.
(25) Li, J.; Ghoshal, S.; Bates, M. K.; Miller, T. E.; Davies, V.; Stavitski, E.; Attenkofer, K.; Mukerjee, S.; Ma, Z.-F.; Jia, Q. Experimental Proof of the Bifunctional Mechanism for the Hydrogen Oxidation in Alkaline Media. *Angew. Chem., Int. Ed.* **2017**, *56*, 15594−15598.
(26) Ünlü, M.; Abbott, D.; Ramaswamy, N.; Ren, X.; Mukerjee, S.; Kohl, P. A. Analysis of Double Layer and Adsorption Effects at the Alkaline Polymer Electrolyte-Electrode Interface. *J. Electrochem. Soc.* **2011**, *158*, B1423−B1431.
(27) Asakura, K.; Kubota, T.; Chun, W. J.; Iwasawa, Y.; Ohtani, K.; Fujikawa, T. Pt L_3-Edge XANES Studies about the Hydrogen Adsorption on small Pt Particles. *J. Synchrotron Radiat.* **1999**, *6*, 439−441.
(28) Kubota, T.; Asakura, K.; Ichikuni, N.; Iwasawa, Y. A New Method for Quantitative Characterization of Adsorbed Hydrogen on Pt Particles by Means of Pt L-edge XANES. *Chem. Phys. Lett.* **1996**, *256*, 445−448.
(29) Árnadóttir, L.; Stuve, E. M.; Jónsson, H. Adsorption of Water Monomer and Clusters on Platinum(111) Terrace and Related Steps and Kinks: I. Configurations, Energies, and Hydrogen Bonding. *Surf. Sci.* **2010**, *604*, 1978−1986.
(30) Sheng, W.; Zhuang, Z.; Gao, M.; Zheng, J.; Chen, J. G.; Yan, Y. Correlating Hydrogen Oxidation and Evolution Activity on Platinum at Different pH with Measured Hydrogen Binding Energy. *Nat. Commun.* **2015**, *6*, 1−6.
(31) Van der Niet, M. J.; Garcia-Araez, N.; Hernández, J.; Feliu, J. M.; Koper, M. T. Water Dissociation on Well-Defined Platinum Surfaces: The Electrochemical Perspective. *Catal. Today* **2013**, *202*, 105−113.
(32) Dubouis, N.; Serva, A.; Salager, E.; Deschamps, M.; Salanne, M.; Grimaud, A. The Fate of Water at the Electrochemical Interfaces: Electrochemical Behavior of Free Water Versus Coordinating Water. *J. Phys. Chem. Lett.* **2018**, *9*, 6683−6688.
(33) Ledezma-Yanez, I.; Wallace, W. D. Z.; Sebastián-Pascual, P.; Climent, V.; Feliu, J. M.; Koper, M. T. M. Interfacial Water Reorganization as a pH-Dependent Descriptor of the Hydrogen Evolution Rate on Platinum Electrodes. *Nat. Energy* **2017**, *2*, 17031.
(34) Herrero, E.; Franaszczuk, K.; Wieckowski, A. Electrochemistry of Methanol at Low Index Crystal Planes of Platinum: An Integrated Voltammetric and Chronoamperometric Study. *J. Phys. Chem.* **1994**, *98*, 5074−5083.
(35) Schwarz, K.; Xu, B.; Yan, Y.; Sundararaman, R. Partial Oxidation of Step-Bound Water Leads to Anomalous pH Effects on Metal Electrode Step-Edges. *Phys. Chem. Chem. Phys.* **2016**, *18*, 16216−16223.
(36) Rheinlander, P.; Henning, S.; Herranz, J.; Gasteiger, H. A. Gasteiger Comparing Hydrogen Oxidation and Evolution Reaction Kinetics on Polycrystalline Platinum in 0.1 and 1 M KOH. *ECS Trans.* **2013**, *50*, 2163−2174.
(37) Shao, M.; Peles, A.; Shoemaker, K. Electrocatalysis on Platinum Nanoparticles: Particle Size Effect on Oxygen Reduction Reaction Activity. *Nano Lett.* **2011**, *11*, 3714−3719.
(38) Liu, E.; Jiao, L.; Li, J.; Stracensky, T.; Sun, Q.; Mukerjee, S.; Jia, Q. Interfacial Water Shuffling the Intermediates of Hydrogen Oxidation and Evolution Reactions in Aqueous Media. *Energy Environ. Sci.* **2020**. DOI: 10.1039/D0EE01754J, in press.
(39) McCrum, I. T.; Hickner, M. A.; Janik, M. J. Quaternary Ammonium Cation Specific Adsorption on Platinum Electrodes: A Combined Experimental and Density Functional Theory Study. *J. Electrochem. Soc.* **2018**, *165*, F114−F121.
(40) Chung, H. T.; Choe, Y.-K.; Martinez, U.; Dumont, J. H.; Mohanty, A.; Bae, C.; Matanovic, I.; Kim, Y. S. Effect of Organic Cations on Hydrogen Oxidation Reaction of Carbon Supported Platinum. *J. Electrochem. Soc.* **2016**, *163*, F1503−F1509.
(41) Kocha, S. S.; Shinozaki, K.; Zack, J. W.; Myers, D. J.; Kariuki, N. N.; Nowicki, T.; Stamenkovic, V.; Kang, Y.; Li, D.; Papageorgopoulos, D. Best Practices and Testing Protocols for Benchmarking ORR Activities of Fuel Cell Electrocatalysts Using Rotating Disk Electrode. *Electrocatalysis* **2017**, *8*, 366−374.
(42) Arruda, T. M.; Shyam, B.; Lawton, J. S.; Ramaswamy, N.; Budil, D. E.; Ramaker, D. E.; Mukerjee, S. Fundamental Aspects of Spontaneous Cathodic Deposition of Ru onto Pt/C Electrocatalysts and Membranes under Direct Methanol Fuel Cell Operating Conditions: an In Situ X-ray Absorption Spectroscopy and Electron Spin Resonance Study. *J. Phys. Chem. C* **2010**, *114*, 1028−1040.
(43) Newville, M. IFEFFIT: Interactive XAFS Analysis and FEFF Fitting. *J. Synchrotron Radiat.* **2001**, *8*, 322−324.
(44) Ravel, B.; Gallagher, K. Atomic Structure and the Magnetic Properties of Zr-Doped Sm2Co17. *Phys. Scr.* **2005**, *2005*, 606.
(45) Newville, M.; Livins, P.; Yacoby, Y.; Rehr, J. J.; Stern, E. A. Near-Edge X-Ray-Absorption Fine Structure of Pb: A Comparison of Theory and Experiment. *Phys. Rev. B: Condens. Matter Mater. Phys.* **1993**, *47*, 14126.
(46) Ankudinov, A. L.; Ravel, B.; Rehr, J. J.; Conradson, S. D. Real-Space Multiple-Scattering Calculation and Interpretation of X-Ray-Absorption Near-Edge Structure. *Phys. Rev. B: Condens. Matter Mater. Phys.* **1998**, *58*, 7565−7576.
(47) Jia, Q.; Li, J.; Caldwell, K.; Ramaker, D. E.; Ziegelbauer, J. M.; Kukreja, R. S.; Kongkanand, A.; Mukerjee, S. Circumventing Metal Dissolution Induced Degradation of Pt-Alloy Catalysts in Proton Exchange Membrane Fuel Cells: Revealing the Asymmetric Volcano Nature of Redox Catalysis. *ACS Catal.* **2016**, *6*, 928−938.